

II. Plasma Instability in Hall Thrusters: Numerical Study

JOVI K

SEM 8, PHYSICS
UM-DAE-CEBS

Project Guide: Dr. Bhooshan Paradkar

Keywords: Plasma Instabilities ♦ Hall Thrusters ♦ Modified Two Fluid Instability ♦
Ion Acoustic Instability ♦ Electron Cyclotron Drift Instability ♦
Electrostatic Dispersion Relation ♦

Department of Physics,
University of Mumbai - Department of Atomic Energy -
Centre for Excellence in Basic Sciences



Certificate

This is to certify that CEBS student **Mr. JOVI K, P0181214** has undertaken project work from 10 Jan 2023 to 30 April 2023 under the guidance of Dr. Bhooshan Paradkar, UM-DAE CEBS.

This submitted project report titled **Plasma Instabilities in Hall Thrusters: Numerical Study** is submitted towards the academic requirements of the Int. M.Sc. Physics Course at UM-DAE CEBS, Mumbai.

Jovi K

Name and signature of
Student with date

02/05/2023

Dr. Bhooshan Paradkar

Name and signature of
Advisor with date

Abstract

Hall effect thrusters (HETs) are widely used in space propulsion systems due to their high thrust-to-power ratio, high specific impulse, high efficiency, and simple structure. However, partial plasma confinement is fundamental to Hall Thrusters Physics and leads to a variety of instabilities such as Modified Two Stream Instability and Electron Cyclotron Drift Instability that negatively impact the efficiency and overall performance of the thrusters. In this study, we numerically solve the general dispersion relation for Hall thrusters to better understand these instabilities and improve the design process.

Acknowledgement

I give my deepest thanks to my supervisor Dr. Bhooshan Paradkar for introducing me to this beautiful subject and for being such an unlimited source of inspiration. His guidance helped me in all the time of my project and writing of this report.

I am also indebted to my fellow classmates for their careful reading of an early draft of the manuscript and for their many valuable comments and suggestions that have been incorporated in the text to improve the presentation.

Table of Contents

Abstract	1
Acknowledgement	2
Table of Contents	3
1 Introduction	4
1.1 Hall Thrusters	4
1.2 Fixed point Iteration for Solving numerical equations:	5
2 Hall thruster Dispersion Relation	7
2.1 Problem at hand.....	7
2.2 Derivation	7
2.2.1 First Principal derivation of Velocity –.....	7
2.2.2 Distribution function	8
2.2.3 Perturbation Equations.....	8
2.2.4 Dispersion Relation:	9
2.3 Limiting Cases of Interest	10
2.3.1 Cold Plasma Limit	10
2.3.2 High T Plasma Limit.....	10
2.3.3 Semi Cold Plasma Limit	11
2.4 Kinds of Instability	11
2.4.1 Modified Two Stream Instability –	11
2.4.2 Electron Cyclotron Drift Instability –	12
3 Numerical Analysis	14
3.1 Normalizing the General Dispersion Relation.....	14
3.2 Numerical solution for the cold ion plasma limit	15
3.2.1 Iterative expression for this case:.....	15
3.3 Numerical solutions –	16
3.3.1 Ducrocq Eq.–.....	17
3.3.2 Modified Ducrocq Eq.–.....	18
3.3.3 General Dispersion relation -	18
3.4 Further prospects	25
4 Bibliography	26

1 Introduction

Partially magnetised plasmas immersed in crossed $E \times B$ fields are employed in electric propulsion systems like Hall thrusters. Such plasmas are prone to a variety of instabilities that impair device operation, particularly instabilities that result in anomalous transport levels that are generally orders of magnitude higher than classical (collisional) transport levels. (Adam, et al., 2008). The nature of anomalous transport (mobility) is yet unknown; however, it has been attributed to several possible instabilities that may interact to produce the observed levels of anomalous transport.

Since this manuscript is more focused on numerical of the general dispersion relation (which was derived by the author in *Plasma Instabilities in Hall Thrusters: Analytical study*¹), the presumed structure of this report is to start with a quick recap of derivation of the general Dispersion relation for Hall Thrusters and three specific cases of interest in [Chapter 2](#), while [Chapter 3](#) consists of the numerical solutions of the Dispersion relation. The manuscript concludes with remarks on how to improve on the work.

1.1 Hall Thrusters

Hall thrusters are gridless ion thrusters used in electric space propulsion systems. Xenon ions are extracted from a plasma without grids and accelerated to around 20 km/s in a conventional Hall thruster working in the kW power range (e.g., 300 V, 4 A), and the thrust is on the order of 70 mN. (Boeuf, 2017; Goebel & Katz, 2008). The strong electric field generated in the quasi-neutral plasma of a Hall thruster accelerates ions due to the loss in electron conductivity caused by the presence of a magnetic barrier perpendicular to the passage of electrons from the cathode to the anode.

Permanent magnets provide this external magnetic barrier. The combination of the parallel electric field E and the perpendicular magnetic field B results in a substantial electron drift in the $E \times B$ direction (Hall current). Good confinement of the electrons and an associated drop of electron conductivity can be achieved only if the Hall current does not hit a wall so the $E \times B$ direction must be closed on itself, i.e., must be in the azimuthal direction of a cylindrical configuration, essentially a closed drift device (Zhurin et al., 1999).

In a Hall thruster, the electric field is axial and the magnetic field is radial (see [Fig. 1-1a](#)). Plasma is produced in a channel between two coaxial dielectric cylinders. Electrons are injected through an emissive cathode outside the exhaust plane, with the anode at the channel's end. The magnetic barrier increases the residence time of electrons in the channel, allowing them to ionise the flow of neutral xenon atoms supplied from the anode. Ionization efficiency is very good in Hall thrusters and more than 90% of the gas flow is ionized for applied voltages on the order of 200 V or more.

A major feature of Hall thrusters is that Ionization occurs immediately upstream of the region of high axial electric field, as can be seen in [Fig. 1-1b](#). Since ions that are essentially unmagnetized, it can

¹ Project and report as part of Semester 8 curriculum

easily be removed from the plasma and accelerated by the axial electric field without colliding as the ionisation and acceleration areas are close together and even overlap. The neutral density in the exhaust section of a Hall thruster is very low due to the high ionisation efficiency, therefore electron movement across magnetic field lines cannot be attributed to electron collisions with neutral atoms. (The neutral density is too low by more than a factor of 10 to allow for classical, collisional cross-field transport, see (Boeuf, 2017)).

Even though Hall thrusters were created over 50 years ago and still used in number of spacecrafts, the electron transport across the magnetic barrier (“anomalous transport”) is still a mystery. Anything ranging from Electron collisions with the channel walls and secondary electron emission to instabilities and turbulence could be responsible for this anomalous transport through the magnetic field.

In recent particle simulations of Hall thrusters, the $E \times B$ Electron Drift Instability ($E \times B$ EDI), also known as Electron Cyclotron Drift Instability, has been identified and is a plausible candidate to explain the electron transport across the magnetic field in these devices. The formation of an azimuthal wave and velocity of the order of the ion acoustic velocity, which promotes electron transport across the magnetic field, characterises this instability.

In 2D geometry, a novel form of unstable mode known as the Modified Two-Stream Instability (MTSI) occurs for finite values of the wave number k_z along the magnetic field. The unstable mode resembles the unmagnetized ion sound at larger values of k_z .

1.2 Fixed point Iteration for Solving numerical equations:

Fixed-point iteration is a numerical method used to solve equations of the form $x = g(x)$ where g is a continuous function. The method starts with an initial guess x_0 for the solution and generates a sequence of approximations x_1, x_2, x_3, \dots using the recursive formula $x_{n+1} = g(x_n)$. The sequence converges to a fixed point of the function g , which is a solution of the equation.

The convergence of the fixed-point iteration method depends on the properties of the function g . If g is Lipschitz continuous with Lipschitz constant $L < 1$, then the fixed-point iteration method converges linearly to the unique fixed point of g . If g is differentiable and its derivative satisfies $|g'(x)| < 1$ for all x in an interval containing the fixed point, then the fixed-point iteration method converges locally to the fixed point.

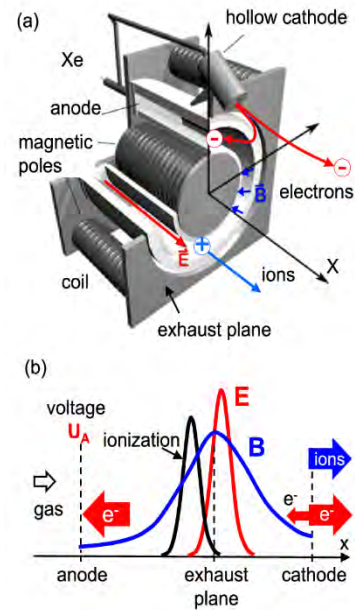


Fig. 1-1: a) Schematic of a Hall thruster. b) The curves show, respectively, the axial profiles along the mid channel axis, of the external radial magnetic field, axial electric field, and ionization rate (number of electron-ion pairs generated per unit volume per unit time).

In practice, the fixed-point iteration method is often used in combination with other numerical methods. For example, it can be used to find an initial guess for Newton's method or to accelerate the convergence of other iterative methods. The choice of the initial guess and the stopping criterion are important factors that affect the performance of the fixed-point iteration method.

Compared to other numerical methods such as Newton's method, fixed-point iteration has its advantages and disadvantages. Newton's method is faster and more robust than fixed-point iteration, as it exploits the information of the derivative of the function f . However, it requires the calculation of f and f' at each iteration, which may be difficult or expensive for some functions. Moreover, it may fail or diverge if f' is zero or close to zero at or near the root.

Here is a summary of other root finding algorithms:

- i. Fixed-point iteration method: This method is used to find the roots of an equation by rewriting it in the form $x = g(x)$. The algorithm then iteratively applies $g(x)$ to an initial guess until convergence is achieved. (John von Neumann, 1929)
- ii. Bisection method: This method is used to find the roots of an equation by repeatedly bisecting an interval and selecting a subinterval in which a root must lie until convergence is achieved. (Thomas Harriot, 1631)
- iii. Newton's method: This method is used to find the roots of an equation by iteratively applying a linear approximation of the function at each guess until convergence is achieved. (Isaac Newton, 1685)
- iv. Secant method: This method is used to find the roots of an equation by iteratively applying a linear approximation of the function using two points until convergence is achieved. (Thomas Simpson, 1740)
- v. False position method: This method is used to find the roots of an equation by iteratively applying a linear approximation of the function using two points until convergence is achieved and then selecting a subinterval in which a root must lie. (Thomas Harriot, 1631)

2 Hall thruster Dispersion Relation

2.1 Problem at hand

The situation is as follows:

1. The instability is studied in the local Cartesian frame depicted because the typical wavelength is short compared to the thruster radius (a few millimetres for a radius of about five centimetres for the thruster used in scattering experiments). Fig. 2-1 is the schematic representation of the model. The \hat{x} axis is along the electric field E_0 and assumed to be along the thruster axis. The \hat{y} axis is locally along the $\mathbf{E} \times \mathbf{B}$ drift velocity V_d and along the azimuthal direction $\hat{\theta}$. The \hat{z} axis is locally along the magnetic field lines in the radial direction. In addition, the plasma is infinite.
2. ions are assumed to be unmagnetized and cold. Landau damping due to ions is neglected.
3. the ion population has a mean velocity $\mathbf{v}_p = v_p \hat{x}$ that is identified as the ion beam/plasma velocity.
4. Dynamics are described using the Vlasov equation. The velocity distribution is assumed to be Maxwellian.
5. the static magnetic field $\mathbf{B}_0 = B_0 \hat{z}$ and the static electric field $\mathbf{E}_0 = E_0 \hat{x}$ are assumed to be uniform. Magnetized electrons drift azimuthally at a velocity $\mathbf{V}_d = -E_0 / B_0 \hat{y}$.
6. the wave is assumed to be electrostatic.

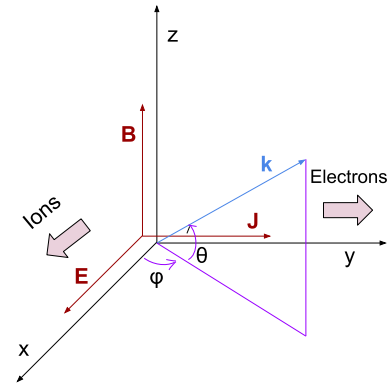


Fig. 2-1: Schematics of the Hall Thruster Problem

2.2 Derivation

In this session we look at the single particle solution in a uniform $\mathbf{E} \times \mathbf{B}$ field. Motivation for a single particle solution is two-fold (i. Integration over unperturbed trajectories using Method of Characteristics; ii. Constants of Motion for the Distribution Function) and is made more apparent in the following sessions. For a detailed derivation refer to *Plasma Instabilities in Hall Thrusters: Analytical study*².

Using Lorentz equation of motion,

$$m\dot{\mathbf{v}} = q(\mathbf{E} + \mathbf{v} \times \mathbf{B}) \text{ where } \mathbf{v} = \mathbf{v}_{\parallel} + \mathbf{v}_{\perp}$$

the most general motion of a charged particle in a uniform field would be,

$$\mathbf{v} = \mathbf{v}_{\parallel} + \mathbf{v}_d + \mathbf{v}_L = \left(\frac{qE_{\parallel}t}{m} + v_0 \right) \hat{\mathbf{B}}_{\parallel} + \frac{\mathbf{E} \times \mathbf{B}}{B^2} + \frac{d[\mathbf{r}_L e^{i\Omega(t-t_0)}]}{dt} \quad (2.2-1)$$

2.2.1 First Principal derivation of Velocity -

For the boundary condition, $\vec{\mathbf{v}}(0) = \hat{\mathbf{v}}_x - E/B \hat{\mathbf{v}}_y + v_{\parallel} \hat{\mathbf{v}}_z$:

² Project and report as part of Semester 8 curriculum

$$\Rightarrow \vec{v}(t) = \cos \omega_{c\sigma} t' \hat{v}_x - [\sin(\omega_{c\sigma} t') + E/B] \hat{v}_y + v_{\parallel} \hat{v}_z$$

Note that this satisfies the ion's case where $\omega_{c\sigma} \rightarrow 0$ and $v_d = 0$ when the ion's motion is physically along x-axis.

2.2.2 Distribution function

We assume a gaussian initial distribution and construct the distribution function using the Constants of Motions, v_{\parallel}^2 and $(v'_{\perp})^2 = (\mathbf{v}_{\perp} - \mathbf{v}_0)^2$,

$$f_{\sigma 0}(\mathbf{v}) = \frac{n_{\sigma 0}}{(2\pi v_{T\sigma}^2)^{3/2}} e^{-\frac{(v_z^2 + v_{\perp}'^2)}{2 v_{T\sigma}^2}} \quad \text{where} \quad v_{T\sigma} = \sqrt{k_B T_{\sigma} / m_{\sigma}} \quad (2.2-2)$$

2.2.3 Perturbation Equations

Under the perturbations,

$$\begin{aligned} \vec{B} &= \mathbf{B} + 0 \\ \vec{E} &= \mathbf{E} - \nabla \phi_1 \quad \text{and} \quad \phi_1 = \tilde{\phi}_1 \exp i[\mathbf{k} \cdot \mathbf{x}(t) - \omega t] \\ f_{\sigma} &= f_{\sigma 0} + f_{\sigma 1} \end{aligned}$$

Using the method of characteristics and Bessel's Identities,

$$f_{\sigma 1}(\mathbf{x}, \mathbf{v}, t) = -\frac{q_{\sigma}}{m_{\sigma} v_{T\sigma}^2} f_{\sigma 0}(\mathbf{v}) \tilde{\phi}_1 e^{i\mathbf{k} \cdot \mathbf{x} - i\omega t} \left[\begin{aligned} &1 + (\omega - \mathbf{k} \cdot \mathbf{v}_0) \sum_{m, n} J_m \left(\frac{k_{\perp} v'_{\perp}}{\omega_{c\sigma}} \right) \\ &\times J_n \left(\frac{k_{\perp} v'_{\perp}}{\omega_{c\sigma}} \right) \frac{e^{i(n-m)\varphi}}{(k_z v_z + k_y v_0 - \omega + n\omega_{c\sigma})} \end{aligned} \right] \quad (2.2-3)$$

where J_n is Bessel's function of first kind.

Perturbation in number density

Since the perturbed number density is,

$$n_{\sigma 1} = \int f_{\sigma 1} d\mathbf{v}$$

And so (note that only k_z comes out of the integral),

$$n_{\sigma 1} = -\frac{q_{\sigma}}{m_{\sigma} v_{T\sigma}^2} \phi_1(\mathbf{x}, t) n_{\sigma 0} \left[1 + \frac{\omega - k_y v_0}{\sqrt{2} k_z v_{T\sigma}} e^{-k_{\perp}^2 r_{L\sigma}^2} \sum_n I_n(k_{\perp}^2 r_{L\sigma}^2) \int_{-\infty}^{\infty} d\xi \frac{e^{-\xi^2}}{\xi - \alpha_{n\sigma}} \right] \quad (2.2-4)$$

where $\alpha_{n\sigma} = (\omega - k_y v_0 - n\omega_{c\sigma}) / \sqrt{2} k_z v_{T\sigma}$ and we have used the Bessel identities.

we have the Ion contribution in the limit $\omega_{ci} \rightarrow 0$ so that $\alpha_{n\sigma} \rightarrow \alpha_{0\sigma}$,

$$n_{i1} = -\frac{en_0}{m_{\sigma} v_{T\sigma}^2} \phi_1(\mathbf{x}, t) \left[1 + \frac{\omega}{\sqrt{2} k_z v_{T\sigma}} Z \left(\frac{\omega}{\sqrt{2} k v_i} \right) \right] \quad (2.2-5)$$

Using Eq. 2.2-4 and 2.2-5 in the Gauss's Law,

$$\nabla^2 \phi_1 = 4\pi(q_i n_i + q_e n_e)$$

We have,

$$\begin{aligned} \frac{k^2 \kappa T_e}{4\pi e^2 n_0} = & -\frac{T_e}{T_i} \left[1 + \frac{\omega}{\sqrt{2} k_z v_{T_i}} Z\left(\frac{\omega}{\sqrt{2} k_z v_{T_i}}\right) \right] \\ & - \left[1 + \frac{(\omega - k_y v_0)}{\sqrt{2} k_z v_{T_e}} \sum_{n=-\infty}^{\infty} e^{-k_{\perp}^2 r_{L\sigma}^2} I_n(k_{\perp}^2 r_{L\sigma}^2) Z\left(\frac{\omega - k_y v_0 - n\omega_{ce}}{\sqrt{2} k_z v_{T_e}}\right) \right] \end{aligned}$$

To get the **warm magnetized plasma** (Doppler shifted electrons) **electrostatic dispersion relation**,

$$\begin{aligned} T_i \left[1 + \frac{k^2 v_{T_e}^2}{\omega_{pe}^2} \right] + T_e \left[1 + \frac{\omega}{\sqrt{2} k_z v_{T_i}} Z\left(\frac{\omega}{\sqrt{2} k_z v_{T_i}}\right) \right] \\ + \frac{(\omega - k_y v_0)}{\sqrt{2} k_z v_{T_e}} \sum_{n=-\infty}^{\infty} e^{-k_{\perp}^2 r_{L\sigma}^2} I_n(k_{\perp}^2 r_{L\sigma}^2) Z\left(\frac{\omega - k_y v_0 - n\omega_{ce}}{\sqrt{2} k_z v_{T_e}}\right) = 0 \end{aligned} \quad (2.2-6)$$

2.2.4 Dispersion Relation:

We define some parameters relevant for our problem,

$$\lambda_D = \sqrt{\frac{\epsilon_0 k_B T_e}{n_e q_e}}, \quad \omega_{p\sigma}^2 = \frac{4\pi n_e q_{\sigma}^2}{m^*}, \quad r_{L\sigma}^2 = \frac{k_B T_{\sigma}}{m_{\sigma} \omega_{c\sigma}^2}, \quad \omega_{c\sigma} = \frac{q_{\sigma} B}{m}, \quad v_{T\sigma} = \sqrt{\frac{k_B T_{\sigma}}{m_{\sigma}}}$$

And the following relation are worth noting,

$$\omega_p \equiv \frac{v_T}{\lambda_D}, \quad \omega_c \equiv \frac{v_T}{r_L}, \quad r_{L\sigma}^2 \equiv \frac{\omega_{p\sigma}^2 \lambda_{D\sigma}^2}{\omega_{c\sigma}^2}$$

where λ_D is the Debye wavelength, ω_p is the plasma frequency, ω_c the cyclotron frequency, v_T is thermal velocity and r_L is the thermal Lamour radius.

This may be compactly written as,

$$1 + k^2 \lambda_{de}^2 + \frac{T_e}{T_i} (1 + \alpha_{0i} Z(\alpha_{0i})) + \alpha_{0e} \sum_{n=-\infty}^{n=\infty} \beta_n Z(\alpha_{ne}) = 0 \quad (2.2-7)$$

where $\alpha_{0i} \equiv \omega/\sqrt{2}k v_{T_i}$ and $\beta_n \equiv e^{-k_y^2 r_e^2} I_n(k_y^2 r_e^2)$ with I_n being n^{th} order modified Bessel function of the first kind, Z is the Fried - Conte function and $\alpha_{ne} \equiv (\omega - k_y v_0 - n\omega_{ce})/\sqrt{2}k_z v_{T_e}$ and r_e is electron Lamour Radius.

Many variations of this Dispersion relation have been intensively studied for e.g., in (Ducrocq et al., 2006) who studied the effects of ion plasma with an initial v_x component or in the context of collisionless plasma shocks by (Gary & Sanderson, 1970) who showed that these resonances become less sharp as the angle θ between the magnetic field and the wave vector decreases and that the growth rate remains high in a small solid angle around $\theta = 90^\circ$ before falling off.

2.3 Limiting Cases of Interest

To be draw any insights from relation we look at various limiting cases. A common formalism in the modern literature is to use the Gordeev integral (Gordeev, 1952) of form,

$$g(\Omega, X, Y) = \frac{\Omega}{\sqrt{2Y}} e^{-X} \sum_{n=-\infty}^{+\infty} Z\left(\frac{\Omega-n}{\sqrt{2Y}}\right) I_n(X)$$

As the asymptotic expansion of this has been obtained using different methods, say, the method of steepest descent as in (Paris, 1998) or a method based on the Hadamard expansion of the Gordeev function as in (Schmitt, 1974). We shall proceed with a method like (Gary, 1970).

These cases are best expressed when we generalize the dispersion relation in the following manner:

$$1 + \sum_{\sigma} \frac{e^{-k_{\perp}^2 r_{L\sigma}^2}}{k^2 \lambda_{D\sigma}^2} \left[I_0(k_{\perp}^2 r_{L\sigma}^2) (1 + \alpha_{0\sigma} Z(\alpha_{0\sigma})) + \sum_{n=1}^{\infty} I_n(k_{\perp}^2 r_{L\sigma}^2) [2 + \alpha_{0\sigma} \{Z(\alpha_{n\sigma}) + Z(\alpha_{-n\sigma})\}] \right] = 0 \quad (2.3-1)$$

- Most general form of **warm magnetized plasma electrostatic dispersion relation** Eq. 2.2-6 for Doppler shifted σ species.
- This form is particularly useful for emphasizing the symmetry in n , which are higher order harmonics of cyclotron frequency.

2.3.1 Cold Plasma Limit

The lowest order thermal correction in the cold plasma limit ($|\alpha_0| \equiv |\omega - k_y v_0|/k_z v_T \gg 1$) is,

$$1 - \frac{k_z^2 \omega_{pi}^2}{k^2 \omega^2} - \frac{e^{-k_{\perp}^2 r_{Le}^2}}{k^2 \lambda_{De}^2} \left[\frac{k_z^2 v_{Te}^2 I_0(k_{\perp}^2 r_{Le}^2)}{(\omega - k_y v_0)^2} - \sum_{n=1}^{\infty} \frac{2n_e^2 \omega_{ce}^2}{(\omega - k_y v_0)^2 - n_e^2 \omega_{ce}^2} I_n(k_{\perp}^2 r_{Le}^2) \right] = 0 \quad (2.3-2)$$

- Notice that the Landau damping appears both at the wave frequency ω and at cyclotron harmonics, i.e., in the vicinity of $n\omega_{c\sigma}$. We shall attempt an analysis of this limit in the following chapter.

2.3.2 High T Plasma Limit

We consider the lowest order thermal correction in the hot plasma limit ($|\alpha_0| \ll 1$),

$$1 + \sum_{\sigma} \frac{e^{-k_{\perp}^2 r_{L\sigma}^2}}{k^2 \lambda_{D\sigma}^2} \left[I_0(k_{\perp}^2 r_{L\sigma}^2) (1 - 2\alpha_{0\sigma}^2 - i\alpha_{0\sigma} \sqrt{\pi}) + 2 \sum_{n=1}^{\infty} I_n(k_{\perp}^2 r_{L\sigma}^2) \left\{ 1 - 2\alpha_{0\sigma}^2 \left(1 - \frac{(\alpha_{n\sigma}^2 + \alpha_{-n\sigma}^2)}{3} \right) + i\alpha_{0\sigma} \sqrt{\pi} \right\} \right] = 0$$

Analyzing this limit is very tricky not only because of the complex dispersion relation but mainly because of the fact that $|\alpha_n| = |(\omega - k_y v_0 - n\omega_{c\sigma})/k_{\parallel} v_{T\sigma}| \ll 1$ happens due to not just $v_{T\sigma} \rightarrow \infty$, but also when $|\omega - k_y v_0| \sim |n\omega_{c\sigma}|$ which leads to strong coupling of electron and ion modes.

Also, in this limit since ions are highly energetic, they can no longer be treated as unmagnetized ($\omega \ll \omega_{ci}$) which is a necessary requirement in Hall Thrusters. This leads us to the next limiting case.

2.3.3 Semi Cold Plasma Limit

A limit that may be of particular importance to Hall Thruster Instabilities is the case when $T_e \gg T_i$ leading to $\alpha_{ne} \ll 1$ and $\alpha_{ni} \gg 1$ expansions in the Dispersion relation.

For $|z| \gg 1$ or $|\frac{\omega - k_x v_p}{\sqrt{2} k_z v_{T_i}}| \gg 1$, when $v_{T_i} \rightarrow 0$,

$$1 + z Z(z) \sim 1 + z \left[i\sqrt{\pi} \sigma e^{-z^2} - \frac{1}{z} \left[1 + \frac{1}{2z^2} + \mathcal{O}(z^{-4}) \right] \right] = iz\sqrt{\pi} \sigma e^{-z^2} - \frac{1}{2z^2} + \mathcal{O}(z^{-4})$$

i.e.,

$$\begin{aligned} 1 + \frac{\omega - k_x v_p}{\sqrt{2} k_z v_{T_i}} Z \left(\frac{\omega - k_x v_p}{\sqrt{2} k_z v_{T_i}} \right) &\sim 1 + \frac{\omega - k_x v_p}{\sqrt{2} k_z v_{T_i}} \left[i\sqrt{\pi} \sigma \exp - \left(\frac{\omega - k_x v_p}{\sqrt{2} k_z v_{T_i}} \right)^2 - \frac{\sqrt{2} k_z v_{T_i}}{\omega - k_x v_p} - \frac{1}{2z^3} \right] \\ &= \frac{i\sqrt{\pi} (\omega - k_x v_p) \sigma}{\sqrt{2} k_z v_{T_i}} \exp - \left(\frac{\omega - k_x v_p}{\sqrt{2} k_z v_{T_i}} \right)^2 - \frac{k_z^2 \lambda_{Di}^2 \omega_{pi}^2}{(\omega - k_x v_p)^2} = X - \frac{k_z^2 \lambda_{Di}^2 \omega_{pi}^2}{(\omega - k_x v_p)^2} \end{aligned}$$

Hence, we have the modified Ducrocq eq.,

$$1 + k^2 \lambda_{De}^2 + g \left(\frac{\omega - k_y V_d}{\omega_{ce}}, (k_x^2 + k_y^2) \rho^2, k_z^2 \rho^2 \right) - \frac{T_e}{T_i} \left[\frac{k^2 \lambda_{Di}^2 \omega_{pi}^2}{(\omega - k_x v_p)^2} - X \right] = 0 \quad (2.3-3)$$

Which in the limit of $X \rightarrow 0$ gives the Ducrocq eq. (Ducrocq et al., 2006),

$$1 + k^2 \lambda_D^2 + g \left(\frac{\omega - k_y V_d}{\omega_{ce}}, (k_x^2 + k_y^2) \rho^2, k_z^2 \rho^2 \right) - \frac{k^2 \lambda_D^2 \omega_{pi}^2}{(\omega - k_x v_p)^2} = 0 \quad (2.3-4)$$

For the numerical analysis in [Chapter 3](#), we shall be starting with this limit since it represents the best of our interest ([Sec. 2.2.1](#)).

2.4 Kinds of Instability

We focus our attention on two basic modes of Instability in the regime of $k_y r_{Le} \ll 1$ or small perturbation wavevector.

2.4.1 Modified Two Stream Instability -

Two Stream Instabilities arise due to interaction among different species that are separated by drift direction and velocity. For the case where $\omega - k_y v_0 \ll \omega_{ce}$ (ions are unmagnetized), $k_y r_{Le} \ll 1$ (so that only the lowest-order finite Larmor radius terms are retained),

For $k_y r_{Le} \ll 1$,

$$\begin{aligned} k_y^2 \left(1 + \frac{r_{Le}^2}{\lambda_{De}^2} - \frac{r_{Li}^2}{\lambda_{Di}^2} \left(\frac{\omega_{ci}^2}{\omega^2} \right) \right) + k_z^2 \left(1 - \frac{1}{\lambda_{De}^2} \left(\frac{v_{Te}^2}{(\omega - k_y v_{e0})^2} \right) - \frac{1}{\lambda_{Di}^2} \frac{v_{Ti}^2}{\omega^2} \right) \\ - k_y^4 \left[\frac{r_{Le}^4}{\lambda_{De}^2} \left(\frac{3}{(4\omega_{ce}^2)} \right) + \frac{r_{Li}^4}{\lambda_{Di}^2} \left(\frac{3\omega_{ci}^2}{(\omega^4)} \right) \right] + k_y^2 k_z^2 \left[\frac{1}{\lambda_{De}^2} \left(\frac{v_{Te}^2 r_{Le}^2}{(\omega - k_y v_{e0})^2} \right) + \frac{1}{\lambda_{Di}^2} \frac{v_{Ti}^2 r_{Li}^2}{\omega^2} \right] = 0 \end{aligned}$$

To fourth order,

$$k_y^2 \left(1 + \frac{\omega_{pe}^2}{\omega_{ce}^2} - \frac{\omega_{pi}^2}{\omega^2} \right) + k_z^2 \left(1 - \frac{\omega_{pe}^2}{(\omega - k_y v_{e0})^2} - \frac{\omega_{pi}^2}{\omega^2} \right) - k_y^4 \left[\frac{3}{4\omega_{ce}^2} \frac{r_{Le}^4}{\lambda_{De}^2} + \frac{3\omega_{ci}^2}{\omega^4} \frac{r_{Li}^4}{\lambda_{Di}^2} \right] + k_y^2 k_z^2 \left[\frac{\omega_{pe}^2 r_{Le}^2}{(\omega - k_y v_{e0})^2} + \frac{\omega_{pi}^2 r_{Li}^2}{\omega^2} \right] = 0 \quad (2.4-1)$$

To second order,

Since $\omega_p \equiv v_T/\lambda_D$ and $\omega_c \equiv v_T/r_L$,

$$k_y^2 \left(1 + \frac{\omega_{pe}^2}{\omega_{ce}^2} - \frac{\omega_{pi}^2}{\omega^2} \right) + k_z^2 \left(1 - \frac{\omega_{pe}^2}{(\omega - k_y v_{e0})^2} - \frac{\omega_{pi}^2}{\omega^2} \right) = 0 \quad (2.4-2)$$

Rewriting this as,

$$1 - \frac{\omega_{pi}^2}{\omega^2} - \frac{\omega_{pe}^2 k_z^2}{(\omega - k_y v_0)^2 k^2} + \frac{\omega_{pe}^2 k_y^2}{\omega_{ce}^2 k^2} = 0$$

This may be thought of as coupling between $\omega^2 \sim \omega_{pi}^2$, and the doppler shifted coupling of electrons,

$$(\omega - k_y v_0)^2 \sim \frac{\omega_{pe}^2 k_z^2}{k_y^2 (\omega_{pe}^2 / \omega_{ce}^2) + k^2}$$

which reduces to the lower electron hybrid mode for $k^2 \sim k_y^2$,

$$(\omega - k_y v_0)^2 \sim \frac{k_z^2}{k_y^2} \left(\frac{1}{\omega_{ce}^2} + \frac{1}{\omega_{pe}^2} \right)^{-1} \equiv \frac{k_z^2}{k_y^2} \omega_{LH}^2$$

The reactive modified two-stream instability changes into the dissipative ion-acoustic instability as the ratio k_z / k_y is increased further. Although this intermediate condition is very hard to be realized analytically, this regime has been investigated by numerical means. It has also been shown that for a large enough $v_{th} k_z / \omega_{ce}$ ratio the dispersion relation approaches that of an ion acoustic wave³ even though the wave vector is almost orthogonal to the magnetic field (Gary & Sanderson, 1970).

2.4.2 Electron Cyclotron Drift Instability –

Due to resonances of the ion-acoustic mode and electron cyclotron harmonics, the electron $E \times B$ flow relative to unmagnetized ions leads to the Electron Cyclotron Drift Instability (ECDI). ECDI is expected to be a key element in creating an electron flow parallel to the background E field at a rate that far exceeds what classical collision theory predicts. Undesirable plasma fluxes towards the walls of $E \times B$ devices may also be a result from such anomalous transport (Wang et al., 2021).

The defining condition for this instability is when $k_{\parallel}/k_{\perp} \ll 1$ leading to the cold plasma, Eq. 2.3-2, we take $k_z \sim 0$,

³ This observation is of particular interest because ion acoustic modes are essentially sound/longitudinal wave perturbations and their existence even though the wavevector is almost perpendicular to perturbation ($\nabla\phi$) requires special attention.

$$k_y^2 \left(1 - \left(\frac{\omega_{pe}^2}{\omega_e^2 - \omega_{ce}^2} \right) - \left(\frac{\omega_{pi}^2}{\omega_i^2 - \omega_{ci}^2} \right) \right) - k_y^4 \left[r_{Le}^2 \left(\frac{3\omega_{pe}^2}{(\omega_e^2 - 4\omega_{ce}^2)(\omega_e^2 - \omega_{ce}^2)} \right) + r_{Li}^2 \left(\frac{3\omega_{pi}^2}{(\omega_i^2 - 4\omega_{ci}^2)(\omega_i^2 - \omega_{ci}^2)} \right) \right] = 0$$

To fourth order,

In the strict limit of $\omega_{ci}^2 \ll \omega^2$,

$$k_y^2 \left(1 - \left(\frac{\omega_{pe}^2}{\omega_e^2 - \omega_{ce}^2} \right) - \left(\frac{\omega_{pi}^2}{\omega_i^2} \right) \right) - k_y^4 \left[r_{Le}^2 \left(\frac{3\omega_{pe}^2}{(\omega_e^2 - 4\omega_{ce}^2)(\omega_e^2 - \omega_{ce}^2)} \right) + 3r_{Li}^2 \frac{\omega_{pi}^2}{\omega_i^4} \right] = 0$$

To second order,

$$k_y^2 \left(1 - \frac{\omega_{pe}^2}{(\omega - k_y v_{e0})^2 - \omega_{ce}^2} - \frac{\omega_{pi}^2}{\omega^2} \right) = 0 \quad (2.4-3)$$

The instability is a result of reactive coupling of the electron (Doppler shifted) upper hybrid mode $(\omega - k v_0)^2 = \omega_{pe}^2 + \omega_{ce}^2$ with the short wavelength ion oscillations $\omega^2 = \omega_{pi}^2$. The contribution of higher $m > 1$ harmonics in Eq. 2.3-1 (which are absent for $T_e = 0$) grows with electron temperature and has the maximum at shorter wavelengths $k_{\perp}^2 r_{Le}^2 \approx 1$ due to the $e^{-k_{\perp}^2 r_{Le}^2} I_n(k_{\perp}^2 r_{Le}^2)$ factors. (Lashmore, D. et al., 1973)

3 Numerical Analysis

3.1 Normalizing the General Dispersion Relation

Normalizing an equation before numerically solving it can improve the accuracy and stability of the numerical solution. Normalization involves scaling the variables and/or coefficients in the equation so that they are of similar magnitude. This can help to avoid issues with numerical precision and round-off errors that can arise when dealing with very large or very small numbers.

Normalization can also be useful when solving systems of equations where the variables have different physical units or scales. By normalizing the variables so that they are dimensionless and of similar magnitude, we can improve the conditioning of the system and make it easier to solve numerically.

We have the general dispersion relation from Eq. 2.2-6,

$$\begin{aligned}
 & 1 + \frac{1}{k^2 \lambda_{Di}^2} \left[1 + \frac{\omega - k_x v_p}{\sqrt{2} k_z v_{Ti}} Z \left(\frac{\omega - k_x v_p}{\sqrt{2} k_z v_{Ti}} \right) \right] \\
 & \quad + \frac{1}{k^2 \lambda_{De}^2} \left[1 + \frac{(\omega - k_y v_0)}{\sqrt{2} k_z v_{Te}} \sum_{n=-\infty}^{\infty} e^{-k_z^2 r_{Le}^2} I_n(k_z^2 r_{Le}^2) Z \left(\frac{\omega - k_y v_0 - n \omega_{ce}}{\sqrt{2} k_z v_{Te}} \right) \right] = 0 \\
 \Rightarrow & 1 + \frac{\lambda_{De}^2}{\hat{k}^2 \lambda_{Di}^2} \left[1 + \frac{(\hat{\omega} - \hat{k}_x \hat{v}_p)/\hat{\omega}_{ci}}{\sqrt{2} k_z r_{Li}} Z \left(\frac{(\hat{\omega} - \hat{k}_x \hat{v}_p)/\hat{\omega}_{ci}}{\sqrt{2} k_z r_{Li}} \right) \right] \\
 & \quad + \frac{1}{\hat{k}^2} \left[1 + \frac{(\hat{\omega} - \hat{k}_x \hat{v}_0)/\hat{\omega}_{ce}}{\sqrt{2} k_z r_{Le}} \sum_{n=-\infty}^{\infty} e^{-k_z^2 r_{Le}^2} I_n(k_z^2 r_{Le}^2) Z \left(\frac{(\hat{\omega} - \hat{k}_x \hat{v}_0)/\hat{\omega}_{ce} - n}{\sqrt{2} k_z r_{Le}} \right) \right] = 0
 \end{aligned}$$

Using,

$$\begin{aligned}
 k_z r_{Li} &= \frac{\hat{k}_z v_{ti}}{\lambda_{De} \omega_{ci}} \frac{\lambda_{Di}}{\lambda_{Di}} = \hat{k}_z \frac{\lambda_{Di}}{\lambda_{De}} = \hat{k}_z \sqrt{\frac{T_i}{T_e}}, & k_z r_{Le} &= \frac{\hat{k}_z v_{te}}{\lambda_{De} \omega_{ce}} = \frac{\hat{k}_z \omega_{pe}/\omega_{pi}}{\omega_{ce}/\omega_{pi}} = \frac{\hat{k}_z}{\hat{\omega}_{ce}} \frac{\omega_{pe}}{\omega_{pi}} = \frac{\hat{k}_z}{\hat{\omega}_{ce}} \sqrt{\frac{m_i}{m_e}} \\
 & 1 + \frac{\lambda_{De}^2}{\hat{k}^2 \lambda_{Di}^2} \left[1 + \frac{(\hat{\omega} - \hat{k}_x \hat{v}_p)/\hat{\omega}_{ci}}{\sqrt{2} \hat{k}_z^2 T_i/T_e} Z \left(\frac{(\hat{\omega} - \hat{k}_x \hat{v}_p)/\hat{\omega}_{ci}}{\sqrt{2} \hat{k}_z^2 T_i/T_e} \right) \right] \\
 & \quad + \frac{1}{\hat{k}^2} \left[1 + \frac{(\hat{\omega} - \hat{k}_x \hat{v}_0)/\hat{\omega}_{ce}}{\sqrt{2} \frac{\hat{k}_z^2 m_i}{\hat{\omega}_{ce}^2 m_e}} e^{-\frac{\hat{k}_z^2 m_i}{\hat{\omega}_{ce}^2 m_e}} \sum_{n=-\infty}^{\infty} I_n \left(\frac{\hat{k}_z^2 m_i}{\hat{\omega}_{ce}^2 m_e} \right) Z \left(\frac{(\hat{\omega} - \hat{k}_x \hat{v}_0)/\hat{\omega}_{ce} - n}{\sqrt{2} \frac{\hat{k}_z^2 m_i}{\hat{\omega}_{ce}^2 m_e}} \right) \right] = 0 \tag{3.1-1}
 \end{aligned}$$

For,

$$\begin{aligned}
 \hat{T} &= \frac{T_i}{T_e}; \quad \hat{M} = \frac{m_i}{m_e} \quad \text{so that} & \Omega_i &= (\hat{\omega} - \hat{k}_x \hat{v}_p)/\hat{\omega}_{ci} & \text{and} & \Omega_e &= (\hat{\omega} - \hat{k}_y \hat{v}_0)/\hat{\omega}_{ce} \\
 & & Y_i &= \hat{k}_z^2 \hat{T} & & X_e &= \frac{\hat{k}_z^2}{\hat{\omega}_{ce}^2} \hat{M} \\
 & & & & & Y_e &= \frac{\hat{k}_z^2}{\hat{\omega}_{ce}^2} \hat{M}
 \end{aligned}$$

We have the warm Hall thruster dispersion relation in normalised form as,

$$\hat{k}^2 + \frac{1}{\hat{T}} \left[1 + \frac{\Omega_i}{\sqrt{2} Y_i} Z \left(\frac{\Omega_i}{\sqrt{2} Y_i} \right) \right] + [1 + g(\Omega_e, X_e, Y_e)] = 0 \quad (3.1-2)$$

And the corresponding fixed point iterative expression is,

$$\hat{\omega}_{n+1} = - \frac{\hat{\omega}_{ci} \sqrt{2} Y_i \left\{ \hat{T} \left(1 + \hat{k}^2 + g(\Omega_{n,e}, X_e, Y_e) \right) + 1 \right\}}{Z \left(\frac{\Omega_{n,i}}{\sqrt{2} Y_i} \right)} + \hat{k}_x \hat{v}_p \quad (3.1-3)$$

3.2 Numerical solution for the cold ion plasma limit

We have the Ducrocq equation, Eq. 2.2-4,

$$1 + k^2 \lambda_D^2 + g \left(\frac{\omega - k_y V_d}{\omega_{ce}}, (k_x^2 + k_y^2) \rho^2, k_z^2 \rho^2 \right) - \frac{k^2 \lambda_D^2 \omega_{pi}^2}{(\omega - k_x v_p)^2} = 0$$

And the corresponding normalised form,

$$1 + \hat{k}^2 + g \left(\frac{\hat{\omega} - \hat{k}_y \hat{V}_d}{\hat{\omega}_{ce}}, (\hat{k}_x^2 + \hat{k}_y^2) \frac{\hat{M}}{\hat{\omega}_{ce}^2}, \hat{k}_z^2 \frac{\hat{M}}{\hat{\omega}_{ce}^2} \right) - \frac{\hat{k}^2}{(\hat{\omega} - \hat{k}_x \hat{v}_p)^2} = 0 \quad (3.2-1)$$

3.2.1 Iterative expression for this case:

Writing it in Normalised terms,

$$(\omega - k_x v_p)^2 = \frac{k^2}{1 + k^2 + g} \quad \text{where } g = g_r + i g_i$$

Solving this we have,

$$\omega_{\pm} = k_x v_p \pm \frac{k}{\sqrt{1 + k^2 + i g_i + g_r}} = k_x v_p \pm \frac{k \sqrt{1 + k^2 - i g_i + g_r}}{\sqrt{g_i^2 + (1 + k^2 + g_r)^2}}$$

To separate the real and the imaginary part we write it in the form,

$$\omega_{\pm} = k_x v_p \pm \frac{k}{\sqrt{g_i^2 + (1 + k^2 + g_r)^2}} (a + ib) \quad (3.2-2)$$

where $a, b \in \mathbb{R}$.

i.e.,

$$a + ib = \sqrt{h - i g_i} \quad \Rightarrow \quad \begin{aligned} h &= a^2 - b^2 \\ b &\rightarrow -\frac{g_i}{2a} \end{aligned}$$

where $h = 1 + k^2 + g_r$.

And so,

$$a_{\mp}^{(+)} = \mp \frac{1}{\sqrt{2}} \sqrt{h + \sqrt{g_i^2 + h^2}} \quad \text{and} \quad b_{\mp}^{(+)} = \pm \frac{g_i}{\sqrt{2} \sqrt{h + \sqrt{g_i^2 + h^2}}}$$

$$a_{\mp}^{(-)} = \mp \frac{1}{\sqrt{2}} \sqrt{h - \sqrt{g_i^2 + h^2}} \quad \text{and} \quad b_{\mp}^{(-)} = \pm \frac{g_i}{\sqrt{2} \sqrt{h - \sqrt{g_i^2 + h^2}}}$$

Since $a, b \in \mathbb{R} \Rightarrow a_{\mp}^{(-)}$ and $b_{\mp}^{(-)}$ are NOT valid solutions.

Substituting (3) in (1) and on simplifying,

$$\omega_{\pm}^{(+)} = k_x v_p \pm \frac{k}{\sqrt{2}} \frac{\left(h + \sqrt{h^2 + g_i^2}\right)^{1/2}}{\sqrt{h^2 + g_i^2}} \mp \frac{i}{\sqrt{2}} \frac{k g_i}{\sqrt{h^2 + g_i^2} \left(h + \sqrt{h^2 + g_i^2}\right)^{1/2}}$$

To get,

$$\omega_{\pm}^{(+)} = k_x v_p \pm \frac{k}{\sqrt{2}} \frac{\left(h + \sqrt{h^2 + g_i^2}\right)^{1/2}}{\sqrt{h^2 + g_i^2}} \mp \frac{i}{\sqrt{2}} \frac{k g_i \left(\sqrt{h^2 + g_i^2} - h\right)^{1/2}}{\sqrt{g_i} \sqrt{h^2 + g_i^2}}$$

The iterative solution then becomes,

$$\begin{aligned} \omega_{+,n+1}^{(+)} &\equiv \hat{\omega}_{+,n+1} = \hat{k}_x \hat{v}_p + \hat{\omega}_{r,n+1} + i\epsilon \hat{\gamma}_{n+1} & \text{where} & \hat{\omega}_{r,n+1} = \frac{1}{\sqrt{2}} \frac{\hat{k}}{\sqrt{h_n^2 + g_{in}^2}} \left(h_n + \sqrt{h_n^2 + g_{in}^2}\right)^{1/2} \\ \omega_{-,n+1}^{(+)} &\equiv \hat{\omega}_{-,n+1} = \hat{k}_x \hat{v}_p - \hat{\omega}_{r,n+1} - i\epsilon \hat{\gamma}_{n+1} & & \hat{\gamma}_{n+1} = \frac{1}{\sqrt{2}} \frac{\hat{k}}{\sqrt{h_n^2 + g_{in}^2}} \left(-h_n + \sqrt{h_n^2 + g_{in}^2}\right)^{1/2} \end{aligned} \quad (3.2-3)$$

is the fixed-point iteration for $h_n = 1 + \hat{k}^2 + g_{rn}$.

The real and imaginary part of the Gordeev function $g\left(\left(\hat{\omega}_n - \hat{k}_y \hat{v}_d\right) / \hat{\omega}_{ce}, \left(\hat{k}_x^2 + \hat{k}_y^2\right) \hat{M} / \hat{\omega}_{ce}^2, \hat{k}_z^2 \hat{M} / \hat{\omega}_{ce}^2\right)$ are g_{rn} and g_{in} , respectively and ϵ is the sign of $-g_{in}$. The process is repeated until convergence error of 10^{-8} is reached (Cavalier et al., 2013).

3.3 Numerical solutions –

And using the normalisations,

M_i (kg)	E_0 (V/m)	B_0 (T)	n_e (m^{-3})	T_e (eV)	v_p (m/s)	T_i (eV)
2.2×10^{-25}	1×10^4	15×10^{-3}	2×10^{17}	25	16,000	10

TABLE 3-1: Typical parameters at the exit plane of the Snecma 5kW PPSX000VR Hall thruster.

We have the normalised values as,

α	\hat{k}_\perp	\hat{k}_z	\hat{v}_p	\hat{V}_d	$\hat{v}_{th,e}$	$\hat{\omega}_{ce}$	\hat{M}
$0^\circ - 360^\circ$	$0 - 2$	0.045	3	150	491	50	2.4×10^5

TABLE 3-3: Typical normalized parameters used to calculate the angular frequency of the modes.

λ_D (m)	ω_{pi} (rad/s)	c_s (m/s)
8.3×10^{-5}	5.1×10^7	4270

TABLE 3-2: Values of the three parameters used for the normalization calculated from Table 3-1

The graphs are plotted in a new normalizing with the normalization factor being,

$$k_0 = \frac{\omega_{ce}}{V_d} \quad \text{and} \quad k/\lambda_D = 0.324 k/k_0$$

where k_0 is called the fundamental resonance wavenumber (Villafana et al., 2021).

3.3.1 Ducrocq Eq.-

We have from Eq. 2.3-4,

$$1 + k^2 \lambda_D^2 + g \left(\frac{\omega - k_y V_d}{\omega_{ce}}, (k_x^2 + k_y^2) \rho^2, k_z^2 \rho^2 \right) - \frac{k^2 \lambda_D^2 \omega_{pi}^2}{(\omega - k_x v_p)^2} = 0$$

And its normalised iterative expression from Eq. 3.2-1 is,

$$(\hat{\omega}_{n+1} - \hat{k}_x \hat{v}_p)^2 = \hat{k}_z^2 / \left(1 + \hat{k}^2 + g \left(\frac{\hat{\omega}_n - \hat{k}_y \hat{V}_d}{\hat{\omega}_{ce}}, (\hat{k}_x^2 + \hat{k}_y^2) \frac{\hat{M}}{\hat{\omega}_{ce}^2}, \hat{k}_z^2 \frac{\hat{M}}{\hat{\omega}_{ce}^2} \right) \right) \quad (3.3-1)$$

Heatmaps in Fig. 3-1 studies the effect of varying α , the angle between \hat{k}_x and \hat{k}_y components. The influence of \hat{k}_z is studied by plotting the normalized angular frequency and growth rate against \hat{k}_y in Fig. 3-2. For the lowest value of \hat{k}_z , sharp resonances are visible on both curves for all \hat{k}_x with lower values being dominant. The growth rate is nearly zero except when $\hat{k}_y V_d$ is close to a cyclotron harmonic. Six peaks are visible on the dispersion relation for $k_y / k_0 \in [0, 5.5]$ or $k_y / \lambda_D \in [0, 1.8]$, consistent with (Gary, 1970). The amplitude of the peaks increases with \hat{k}_y until it reaches ~ 1 . Increasing \hat{k}_z smoothes the curves and the resonances are less visible. For a given \hat{k}_z , increasing \hat{k}_x has a similar effect. For high values of \hat{k}_z , no more resonances are visible and both curves seem to be an average of the profiles at lower \hat{k}_z . For higher values of \hat{k}_z , the dispersion relations no longer changes. For any value of \hat{k}_z , for low values of \hat{k}_y the dispersion relation does not go to zero but to \hat{k}_\perp . For high values of \hat{k}_y , the normalized angular frequency approaches ~ 1 .

From the analysis of Sec. 2.4, it may be inferred that the first mode at $\hat{k}_y \sim 1$ corresponds to MTSI while all other modes correspond to ECDI.

3.3.2 Modified Ducrocq Eq.-

The modified Ducrocq equation Eq. 2.3-3,

$$1 + k^2 \lambda_{De}^2 + g \left(\frac{\omega - k_y V_d}{\omega_{ce}}, (k_x^2 + k_y^2) \rho^2, k_z^2 \rho^2 \right) - \frac{T_e}{T_i} \left[\frac{k^2 \lambda_{Di}^2 \omega_{pi}^2}{(\omega - k_x v_p)^2} - X \right] = 0$$

$$\text{where } X = \frac{i\sqrt{\pi}(\omega - k_x v_p)\sigma}{\sqrt{2}k_z v_{Ti}} \exp - \left(\frac{\omega - k_x v_p}{\sqrt{2}k_z v_{Ti}} \right)^2$$

While the normalised iterative form is,

$$\begin{aligned} & (\hat{\omega}_{n+1} - \hat{k}_x \hat{v}_p)^2 \\ & = \hat{k}^2 / \left[1 + \hat{k}^2 + g \left(\frac{\hat{\omega}_n - \hat{k}_y \hat{V}_d}{\hat{\omega}_{ce}}, (\hat{k}_x^2 + \hat{k}_y^2) \frac{\hat{M}}{\hat{\omega}_{ce}^2}, \hat{k}_z^2 \frac{\hat{M}}{\hat{\omega}_{ce}^2} \right) + \frac{i\sqrt{\pi}\sigma}{\hat{T}} \frac{\Omega_{i,n}}{\sqrt{2} Y_i} \exp - \left(\frac{\Omega_{i,n}}{\sqrt{2} Y_i} \right)^2 \right] \end{aligned} \quad (3.3-2)$$

Here we treat X as a perturbation over the original Ducrocq Equation. For ease of convergence and implementation the solution from the original Ducrocq numerical solution is fed into the perturbation, rather than initializing with a zero-like solution.

The influence of \hat{k}_z is studied by plotting the normalized angular frequency and growth rate against \hat{k}_y in Fig. 3-4. Heatmaps in Fig. 3-3 studies the effect of varying α , the angle between \hat{k}_x and \hat{k}_y components. Here the temperature effects are very visible for lower values of \hat{k} , in particular \hat{k}_y . The same manifest as a small dip for lower \hat{k}_y in the normalised angular frequency plots but has a severe effect in the growth rate where the mode $\hat{k}_y \sim 0.18$ sees a drastic peak for $\hat{k}_x \sim 3$. As was recognised earlier this first peak that is different from other peaks at integer values of \hat{k}_y is the MTSI mode, and predicts a surprisingly high growth of MTSI mode for $\hat{k}_x > 3$.

3.3.3 General Dispersion relation -

The normalised warm Hall thruster dispersion relation, Eq. 2.2-7,

$$\hat{k}^2 + \frac{1}{\hat{T}} \left[1 + \frac{\Omega_i}{\sqrt{2} Y_i} Z \left(\frac{\Omega_i}{\sqrt{2} Y_i} \right) \right] + [1 + g(\Omega_e, X_e, Y_e)] = 0$$

The fixed-point implementation uses Eq. 3.1-3,

$$\hat{\omega}_{n+1} = - \frac{\hat{\omega}_{ci} \sqrt{2} Y_i \left\{ \hat{T} \left(1 + \hat{k}^2 + g(\Omega_{n,e}, X_e, Y_e) \right) + 1 \right\}}{Z \left(\frac{\Omega_{n,i}}{\sqrt{2} Y_i} \right)} + \hat{k}_x \hat{v}_p$$

Heatmaps in Fig. 3-5 identifies the effect of varying α , the angle between \hat{k}_x and \hat{k}_y components. The influence of \hat{k}_z is studied by plotting the normalized angular frequency and growth rate against \hat{k}_y in Fig. 3-6. Although an initial stability analysis of this non-linear equation seems to be consistent, a full-fledged analysis is beyond the scope the manuscript. The result seems to suggest a strong damping for large \hat{k}_y and the damping resonating with higher ECDI for lower \hat{k}_z values.

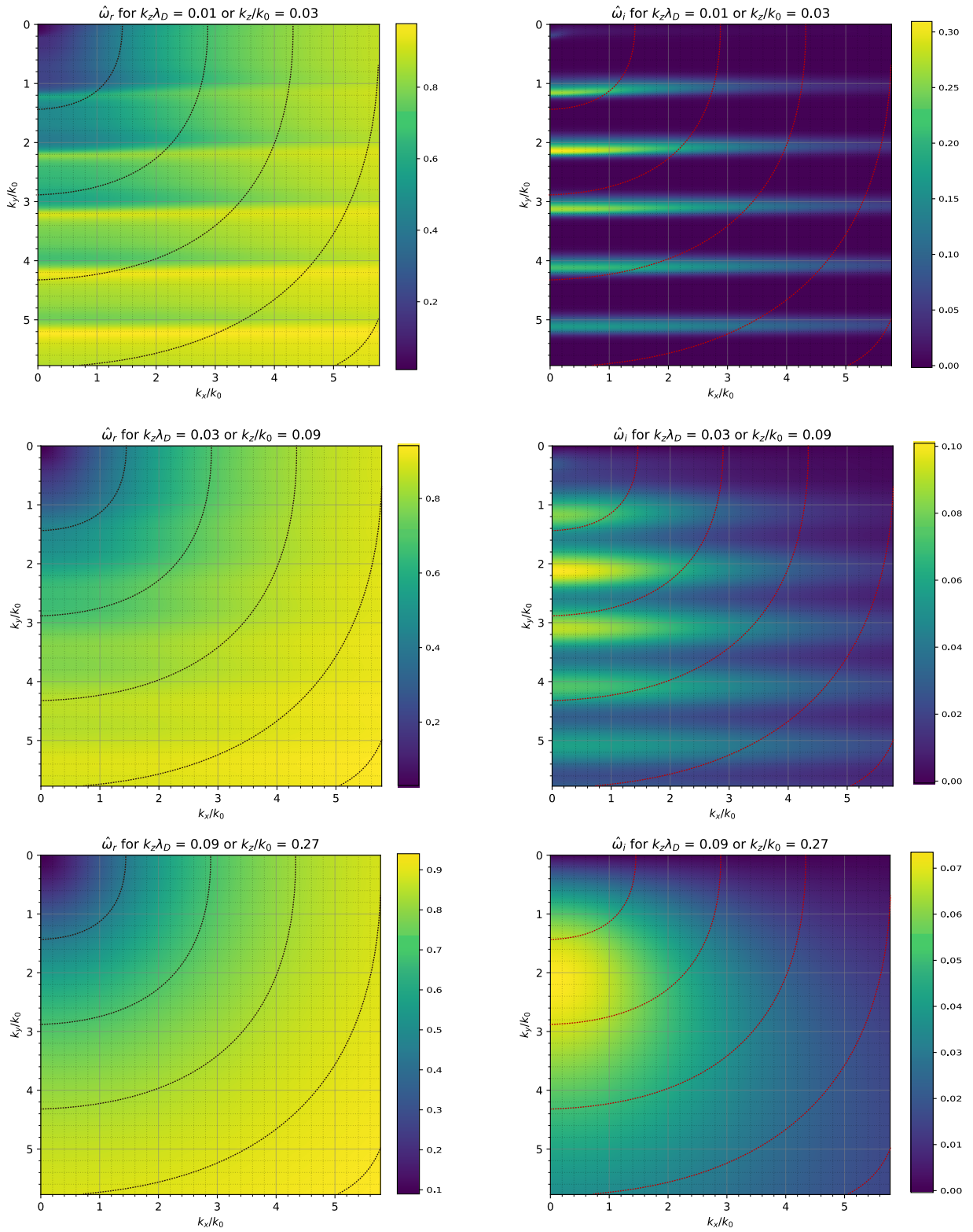


Fig. 3-1: Heatmap of $\hat{\omega}$ vs (\hat{k}_x, \hat{k}_y) for different values of \hat{k}_z of Ducrocq relation, Eq. 3.3-1. Dashed outlines represent contours of $\hat{k}_\perp^2 \equiv \hat{k}_x^2 + \hat{k}_y^2 = \text{const.}$

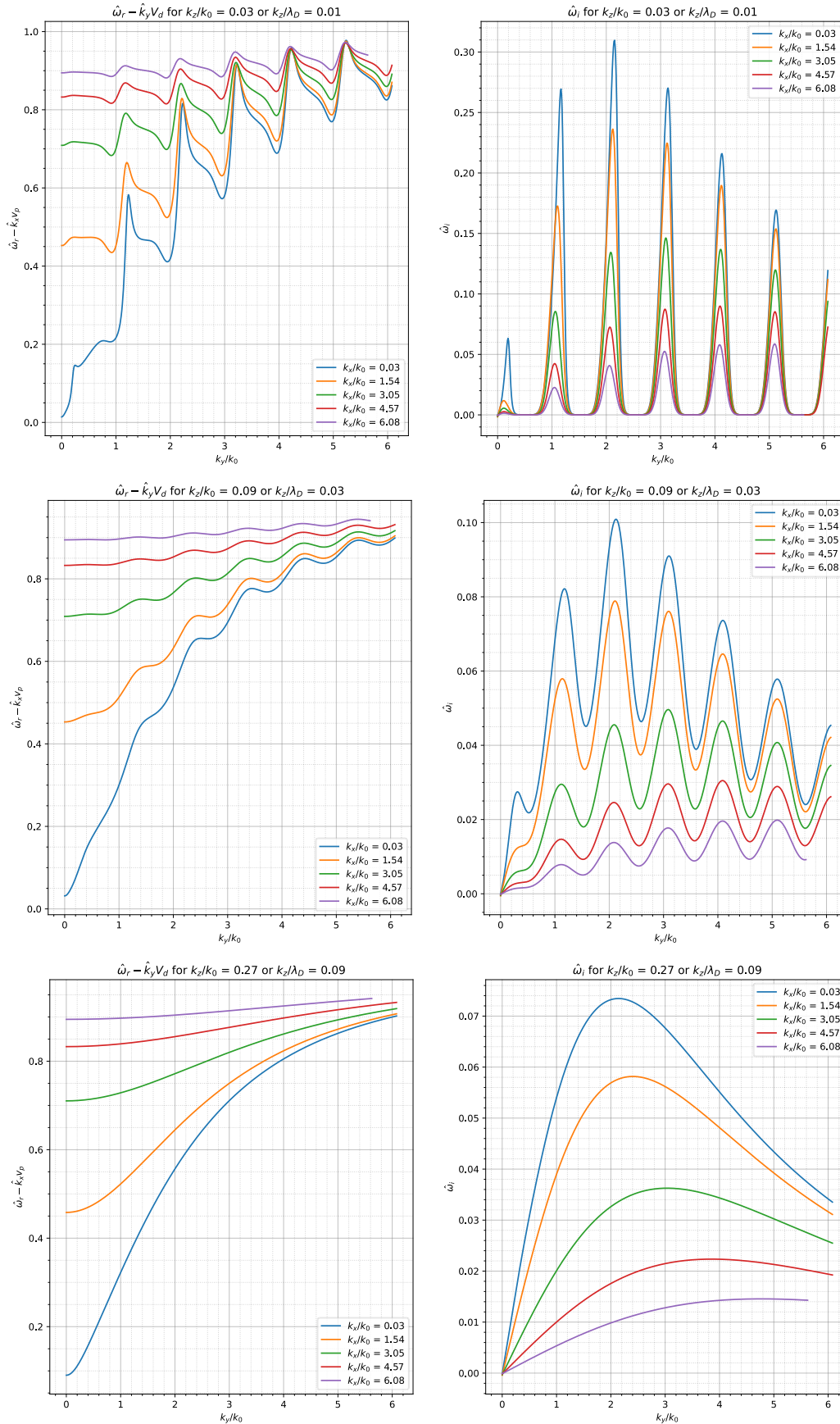


Fig. 3-2: A plot of $\hat{\omega}$ vs (\hat{k}_x, \hat{k}_y) for different values of \hat{k}_z of Ducrocq relation, Eq. 3.3-1. Dashed outlines represent contours of $\hat{k}_\perp^2 \equiv \hat{k}_x^2 + \hat{k}_y^2 = \text{const}$.

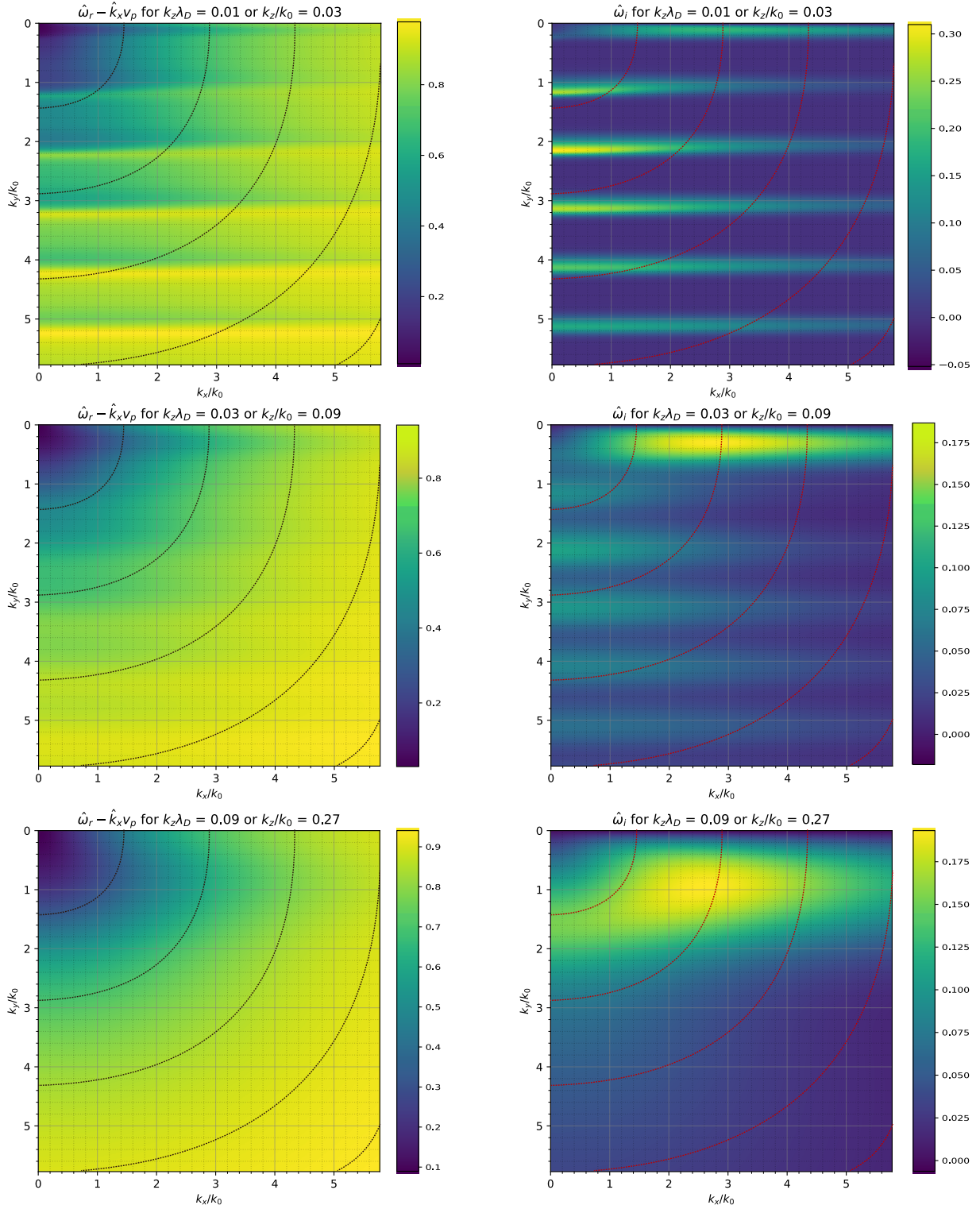


Fig. 3-3: Heatmap of $\hat{\omega}$ vs (\hat{k}_x, \hat{k}_y) for different values of \hat{k}_z of the modified Ducrocq relation, Eq. 3.3-2. Dashed outlines represent contours of $\hat{k}_\perp^2 \equiv \hat{k}_x^2 + \hat{k}_y^2 = \text{const.}$

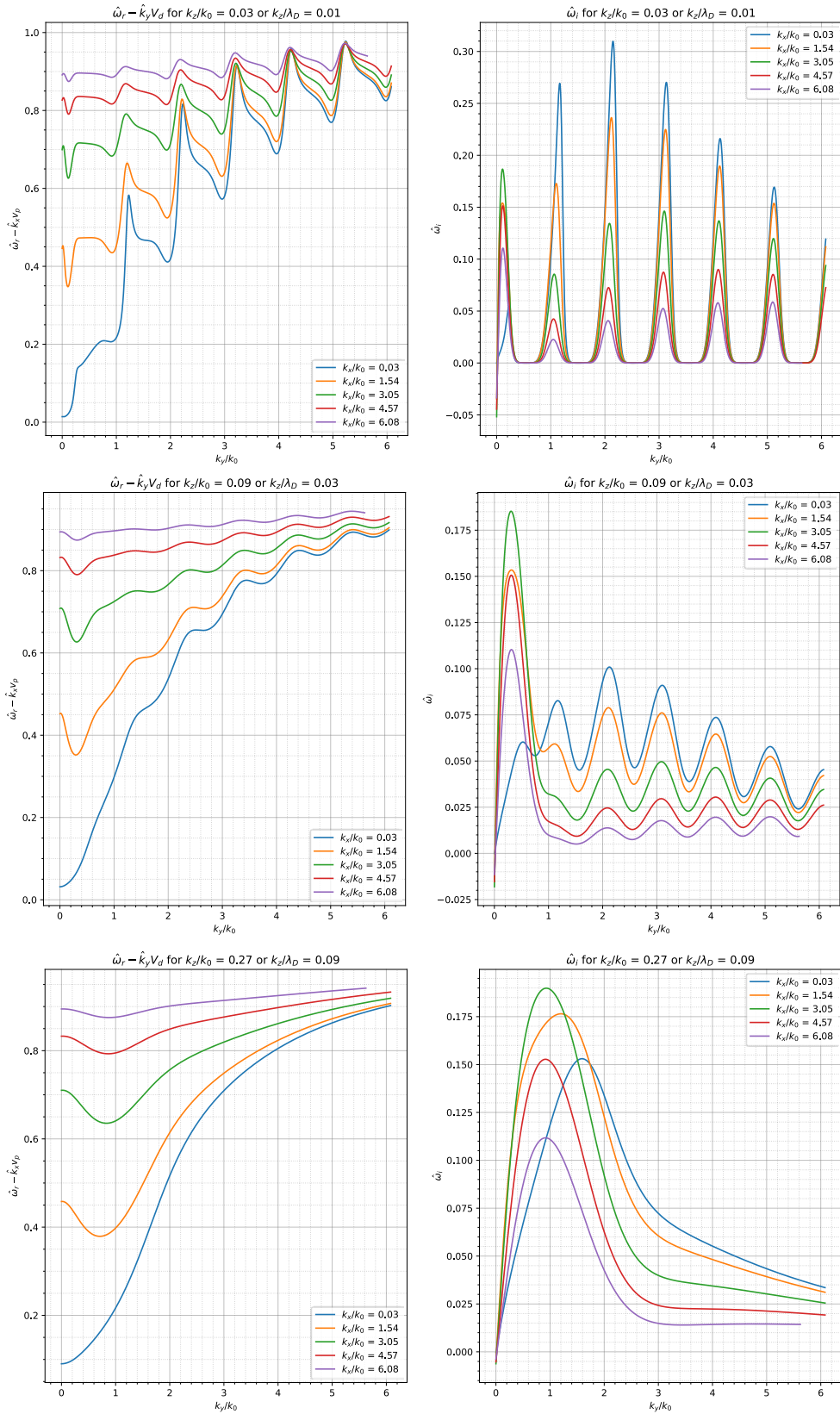


Fig. 3-4: A plot of $\hat{\omega}$ vs (\hat{k}_x, \hat{k}_y) for different values of \hat{k}_z of the modified Ducrocq relation, Eq. 3.3-2. Dashed outlines represent contours of $\hat{k}_\perp^2 \equiv \hat{k}_x^2 + \hat{k}_y^2 = \text{const}$.

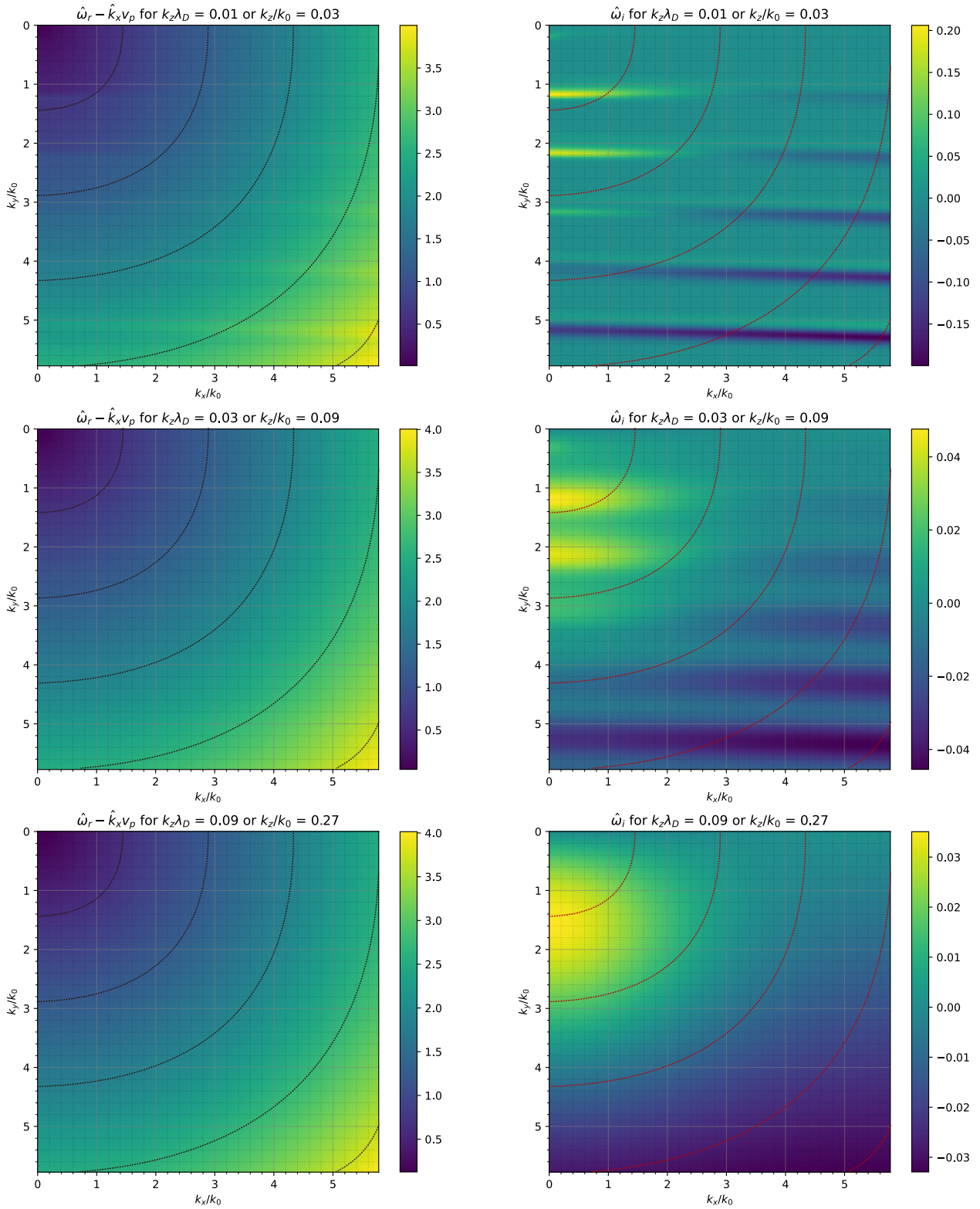


Fig. 3-5: Heatmap of $\hat{\omega}$ vs (\hat{k}_x, \hat{k}_y) for different values of \hat{k}_z of the general dispersion relation, Eq. 3.1-3. Dashed outlines represent contours of $\hat{k}_1^2 \equiv \hat{k}_x^2 + \hat{k}_y^2 = \text{const.}$

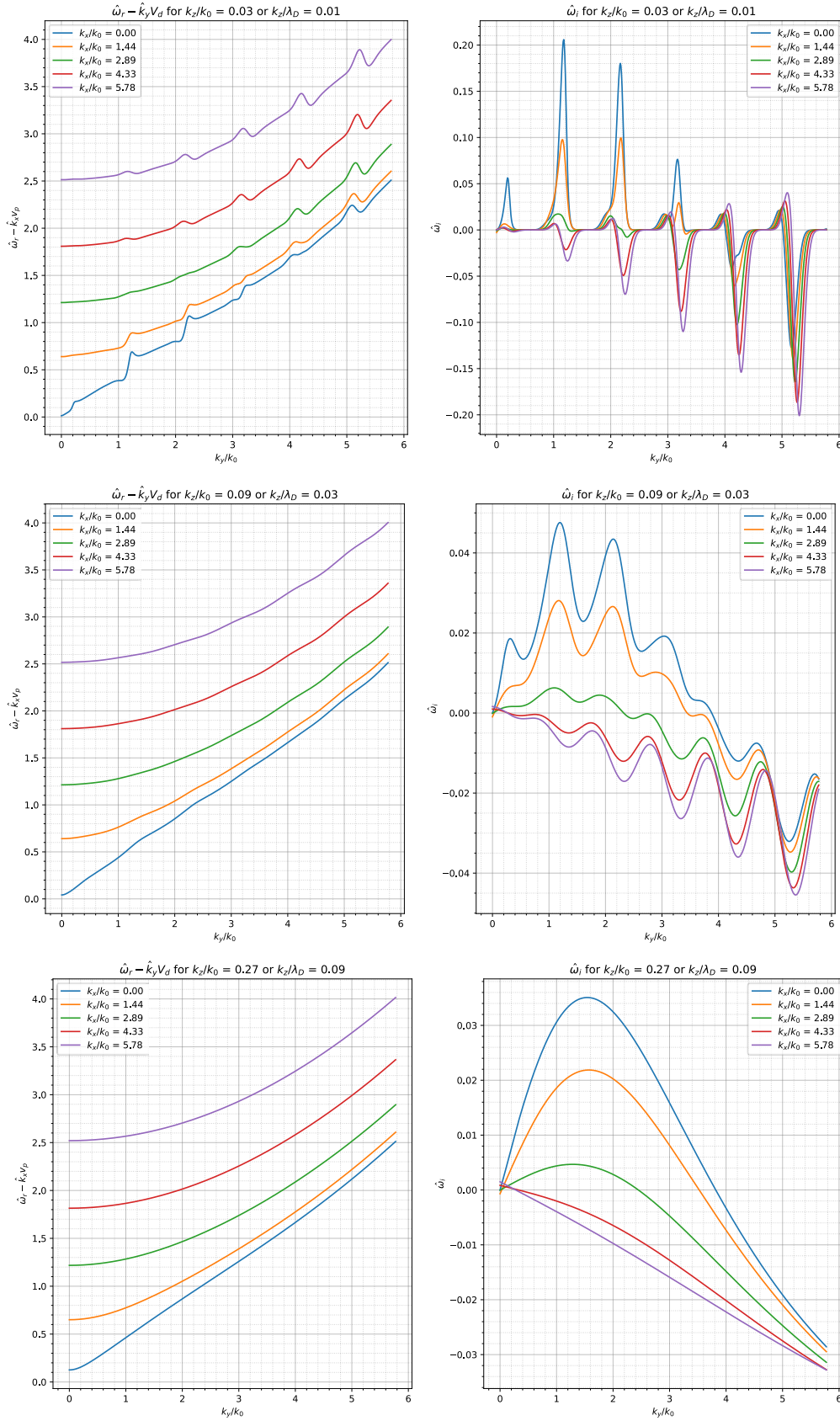


Fig. 3-6: A plot of $\hat{\omega}$ vs (\hat{k}_x, \hat{k}_y) for different values of \hat{k}_z of the general dispersion relation, Eq. 3.1-3. Dashed outlines represent contours of $\hat{k}_\perp^2 \equiv \hat{k}_x^2 + \hat{k}_y^2 = \text{const}$.

3.4 Further prospects

- The dispersion equation for this problem Eq. 2.2-6 was derived assuming that the particles had Maxwellian or shifted Maxwellian velocity distributions. The dissipative instabilities described in this manuscript are all very sensitive to the form of the velocity distribution and may have very different consequences depending on the distribution profile.
- We have neglected the gradient effects for low- β plasma (ratio of electron pressure to magnetic pressure) case where the $E_0 \times B_0$ drift is found to dominate. If the gradient effects are put in, then the electromagnetic terms should also be included.
- A temperature dependence analysis has not been included in this manuscript, which will provide valuable insights into the micro-instabilities at hand.
- The numerical solution of the General dispersion relation requires a much more vigorous take to fully comprehend the analysis.

4 Bibliography

- Boeuf, J. P. (2017). Tutorial: Physics and modelling of Hall thrusters. *Journal of Applied Physics*, *121*(1), 011101. <https://doi.org/10.1063/1.4972269>
- Cavalier, J., Lemoine, N., Bonhomme, G., Tsikata, S., Honoré, C., & Grésillon, D. (2013). Hall thruster plasma fluctuations identified as the E×B electron drift instability: Modelling and fitting on experimental data. *Physics of Plasmas*, *20*(8), 082107. <https://doi.org/10.1063/1.4817743>
- Ducrocq, A., Adam, J. C., Hron, A., & Laval, G. (2006). High-frequency electron drift instability in the cross-field configuration of Hall thrusters. *Physics of Plasmas*, *13*(10), 102111. <https://doi.org/10.1063/1.2359718>
- Gary, S. P. (1970). Longitudinal waves in a perpendicular collisionless plasma shock: II. Vlasov ions. *Journal of Plasma Physics*, *4*(4), 753–760. <https://doi.org/10.1017/S0022377800005407>
- Gary, S. P., & Sanderson, J. J. (1970). Longitudinal waves in a perpendicular collisionless plasma shock: I. Cold ions. *Journal of Plasma Physics*, *4*(4), 739–751. <https://doi.org/10.1017/S0022377800005390>
- Goebel, D. M., & Katz, I. (2008). *Fundamentals of electric propulsion: ion and Hall thrusters*. 507.
- Gordeev, G. v. (1952). Zh. Eksp. Teor. Fiz. (*Sov. Phys.-JETP*), *23*(660).
- Lashmore-Da Vies, C. N., & Martin Ukaea, T. J. (1973). Electrostatic instabilities driven by an electric current perpendicular to a magnetic field. *Nuclear Fusion*, *13*(2), 193. <https://doi.org/10.1088/0029-5515/13/2/007>
- Paris, R. B. (1998). The asymptotic expansion of Gordeyev's integral. *Zeitschrift Für Angewandte Mathematik Und Physik ZAMP 1998 49:2*, *49*(2), 322–338. <https://doi.org/10.1007/PL00001486>
- Schmitt, J. P. M. (1974). The magneto plasma dispersion function: some mathematical properties. *Journal of Plasma Physics*, *12*(1), 51–59. <https://doi.org/10.1017/S0022377800024922>
- Villafana, W., Petronio, F., Denig, A. C., Jimenez, M. J., Eremin, D., Garrigues, L., Taccogna, F., Alvarez-Laguna, A., Boeuf, J. P., Bourdon, A., Chabert, P., Charoy, T., Cuenot, B., Hara, K., Pechereau, F., Smolyakov, A., Sydorenko, D., Tavant, A., & Vermorel, O. (2021). 2D radial-azimuthal particle-in-cell benchmark for E×B discharges. *Plasma Sources Science and Technology*, *30*(7), 075002. <https://doi.org/10.1088/1361-6595/AC0A4A>
- Wang, L., Hakim, A., Srinivasan, B., & Juno, J. (2021). *Electron cyclotron drift instability and anomalous transport: two-fluid moment theory and modelling*. <https://doi.org/10.48550/arxiv.2107.09874>
- Zhurin, V. v., Kaufman, H. R., & Robinson, R. S. (1999). Physics of closed drift thrusters. *Plasma Sources Science and Technology*, *8*(1), R1. <https://doi.org/10.1088/0963-0252/8/1/021>

(This page intentionally left blank)